OPEN ACCESS Freely available online

PLOS ONE

Is Buffer a Good Proxy for a Crowded Cell-Like Environment? A Comparative NMR Study of Calmodulin Side-Chain Dynamics in Buffer and *E. coli* Lysate

Michael P. Latham[1]*, Lewis E. Kay[1,2]*

1 Departments of Molecular Genetics, Biochemistry and Chemistry, The University of Toronto, Toronto, Ontario, Canada, **2** Hospital for Sick Children, Program in Molecular Structure and Function, Toronto, Ontario, Canada

Abstract

Biophysical studies of protein structure and dynamics are typically performed in a highly controlled manner involving only the protein(s) of interest. Comparatively fewer such studies have been carried out in the context of a cellular environment that typically involves many biomolecules, ions and metabolites. Recently, solution NMR spectroscopy, focusing primarily on backbone amide groups as reporters, has emerged as a powerful technique for investigating protein structure and dynamics *in vivo* and in crowded "cell-like" environments. Here we extend these studies through a comparative analysis of Ile, Leu, Val and Met methyl side-chain motions in apo, Ca^{2+}-bound and Ca^{2+}, peptide-bound calmodulin dissolved in aqueous buffer or in *E. coli* lysate. Deuterium spin relaxation experiments, sensitive to pico- to nano-second time-scale processes and Carr-Purcell-Meiboom-Gill relaxation dispersion experiments, reporting on millisecond dynamics, have been recorded. Both similarities and differences in motional properties are noted for calmodulin dissolved in buffer or in lysate. These results emphasize that while significant insights can be obtained through detailed "test-tube" studies, experiments performed under conditions that are "cell-like" are critical for obtaining a comprehensive understanding of protein motion *in vivo* and therefore for elucidating the relation between motion and function.

Citation: Latham MP, Kay LE (2012) Is Buffer a Good Proxy for a Crowded Cell-Like Environment? A Comparative NMR Study of Calmodulin Side-Chain Dynamics in Buffer and *E. coli* Lysate. PLoS ONE 7(10): e48226. doi:10.1371/journal.pone.0048226

Editor: Daniel S. Sem, Concordia University Wisconsin, United States of America

Received July 13, 2012; **Accepted** September 24, 2012; **Published** October 30, 2012

Copyright: © 2012 Latham, Kay. This is an open-access article distributed under the terms of the Creative Commons Attribution License, which permits unrestricted use, distribution, and reproduction in any medium, provided the original author and source are credited.

Funding: M.P.L. acknowledges support in the form of post-doctoral fellowships from the National Science Foundation (OISE-0853108) and the Canadian Institutes of Health Research (CIHR) Training Grant in Protein Folding and Disease. This work was supported by a grant from the CIHR. The funders had no role in study design, data collection and analysis, decision to publish, or preparation of the manuscript.

Competing Interests: The authors have declared that no competing interests exist.

* E-mail: latham@pound.med.utoronto.ca; kay@pound.med.utoronto.ca

Introduction

A clear link has been established between protein structure, dynamics and function through studies using a wide-range of structural, biophysical and biochemical techniques [1–5]. For the most part, however, these studies are performed *in vitro*, using isolated proteins that have been purified to homogeneity so that the effects of the "natural biological environment" are removed. The environment in which a protein functions is a complicated heterogeneous mixture containing as many as 100 million metabolites and 2.4 million proteins per cell [6,7]. This complex milieu can have both stabilizing and destabilizing effects on the constituent proteins. For example, the high concentrations of macromolecules can lead to increased folding propensity due to excluded volume effects, whereas, non-specific associations between macromolecules can potentially result in unfolding [8–15]. Additionally, the kinetics and thermodynamics of interactions can be significantly changed relative to the pristine environment of a test-tube [16–18]. It is clear that an in-depth picture of a protein's structure, dynamics and function must take into account the unique properties that are found in-cell.

Nuclear magnetic resonance (NMR) spectroscopy has emerged as a powerful technique for studying proteins within the biological context of the cellular environment [14,15,19–28]. While the vast majority of *in vivo* or in "cell-like" NMR studies have utilized backbone amide groups as probes of structure and dynamics, hydrophobic methyl containing side-chains could potentially also serve as valuable reporters [26,29]. For example, NMR spectra of methyl groups have signal-to-noise ratios that are significantly higher than amide data sets [26]. Methyl containing side-chains are often localized to protein-protein interfaces, ligand binding pockets, enzyme active sites and the hydrophobic cores of globular proteins and thus provide complementary information to amide groups [30]. The importance of methyl containing residues in facilitating non-specific interactions in the cellular environment has been demonstrated by mutation of a surface hydrophobic patch on the protein ubiquitin, resulting in a significant improvement in *in vivo* NMR spectral quality [21]. This presumably reflects the elimination of transient contacts with one or more native proteins in the cell.

Here we have prepared a series of U-[^{2}H], Ile-δ1[$^{13}CHD_2$]-, Leu,Val-[$^{13}CHD_2$, $^{13}CHD_2$]-, Met[$^{13}CHD_2$]-labeled calmodulin (CaM) samples to study methyl side-chain dynamics in a "cell-like" environment comprising 100 g/L (native protein concentration) *E. coli* lysate (referred to as lysate CaM). ^{2}H-based spin relaxation experiments [31,32] were recorded on Ca^{2+}-free CaM (apoCaM in what follows) as well as Ca^{2+}-loaded CaM in complex with a substrate peptide from smooth muscle myosin light chain kinase, Ca^{2+}-CaM-smMLCK(p). These measurements establish that the amplitude and time-scale of fast (picosecond, ps –nanosecond, ns)

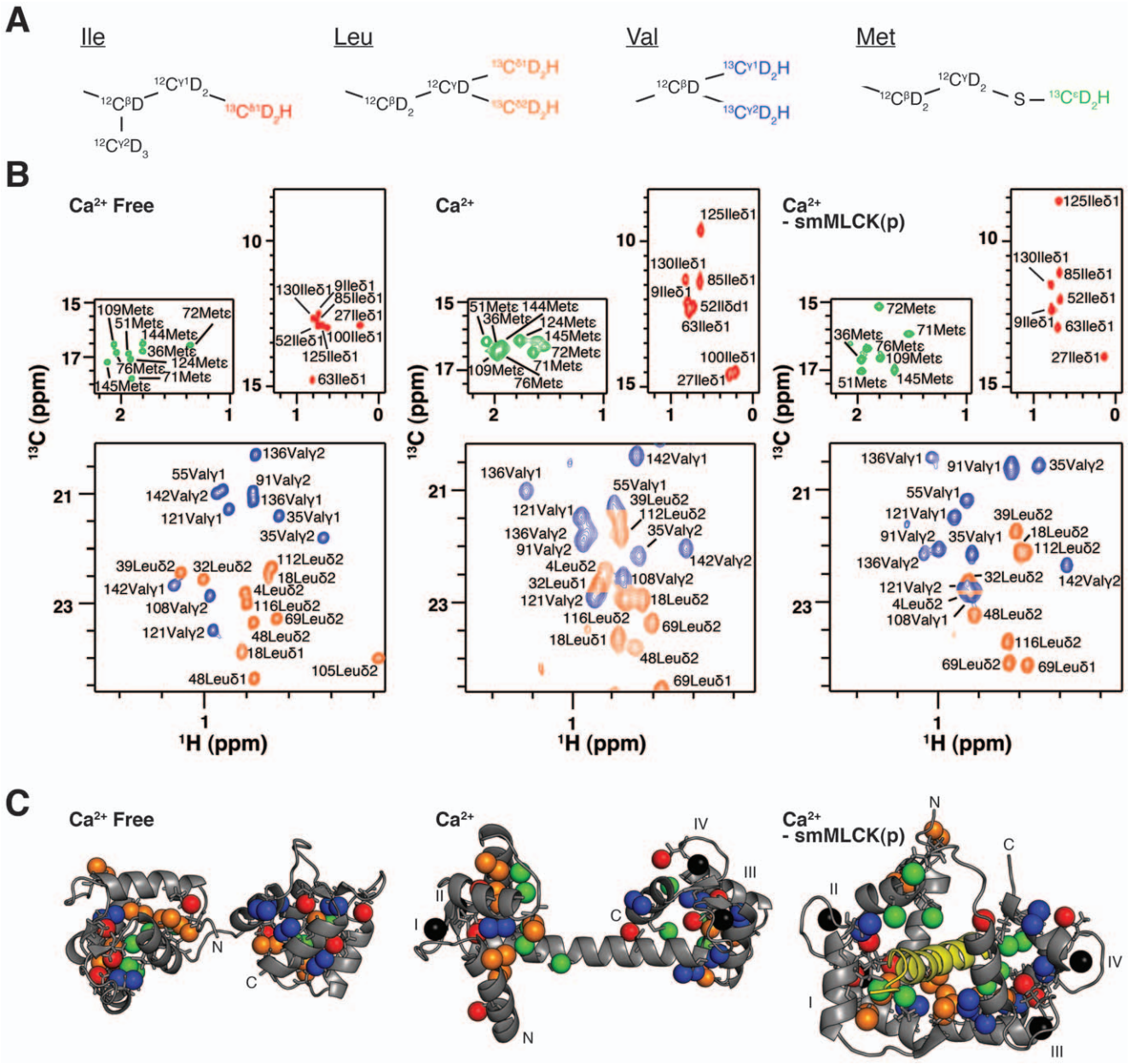

Figure 1. Ile, Leu, Val and Met methyl probes of CaM side-chain dynamics in *E. coli* lysate. (A) $^{13}CHD_2$ labeling scheme for Ileδ1, Leuδ, Valγ and Metε methyl groups. (B) ^{2}H-edited 2D ^{13}C-^{1}H correlation spectra of U-[^{2}H],Ile-δ1[$^{13}CHD_2$]-, Leu,Val-[$^{13}CHD_2$, $^{13}CHD_2$]-, Met[$^{13}CHD_2$]-labeled samples of apoCaM, Ca^{2+}-CaM, and Ca^{2+}-CaM-smMLCK(p) in 100 g/L *E. coli* lysate. Data sets were obtained using a pulse scheme described previously for measurement of ^{2}H T_2 relaxation times with $T = 0$ [32]. Panels show Metε, Ileδ1 and a portion of the Leuδ/Valγ region of each spectrum, with assignment of correlations as indicated. (C) Corresponding structures for the three CaM states with the $^{13}CHD_2$– labeled methyl groups highlighted as spheres: Ileδ1, red; Leuδ, orange; Valγ, blue; Metε, green. An identical color scheme is used in (A) and (B). For the Ca^{2+}-CaM (3CLN) [40] and Ca^{2+}-CaM-smMLCK(p) (2BBM) [42] structures the four Ca^{2+} ions are shown as black spheres and the Ca^{2+} binding sites are labeled. The smMLCK(p) is in yellow for Ca^{2+}-CaM-smMLCK(p). The structure of apoCaM is derived from PDB coordinates 1DMO [38].
doi:10.1371/journal.pone.0048226.g001

methyl side-chain dynamics are very similar in aqueous buffer and under "cell-like" conditions in these two cases. In order to probe millisecond (ms) time-scale motional properties, ^{1}H Carr-Purcell-Meiboom [33,34] (CPMG) relaxation dispersion experiments [35] were recorded on apoCaM, Ca^{2+}-loaded CaM (Ca^{2+}-CaM) and Ca^{2+}-CaM-smMLCK(p) protein states. Striking differences in ms motions were observed for buffer and lysate apoCaM, resulting from sampling of a metal bound intermediate in the lysate environment. Similarly, large differences in dispersion profiles were noted for buffer and lysate Ca^{2+}-CaM, reflecting transient CaM interactions with native proteins in the lysate. By contrast, relaxation dispersion experiments indicate very much reduced ms time-scale dynamics for lysate Ca^{2+}-CaM-smMLCK(p) relative to either lysate apoCaM or lysate Ca^{2+}-CaM. Our results highlight both the similarities and the differences in motional properties of CaM in the two environments and therefore the importance of extending studies of protein structure and dynamics beyond the test-tube.

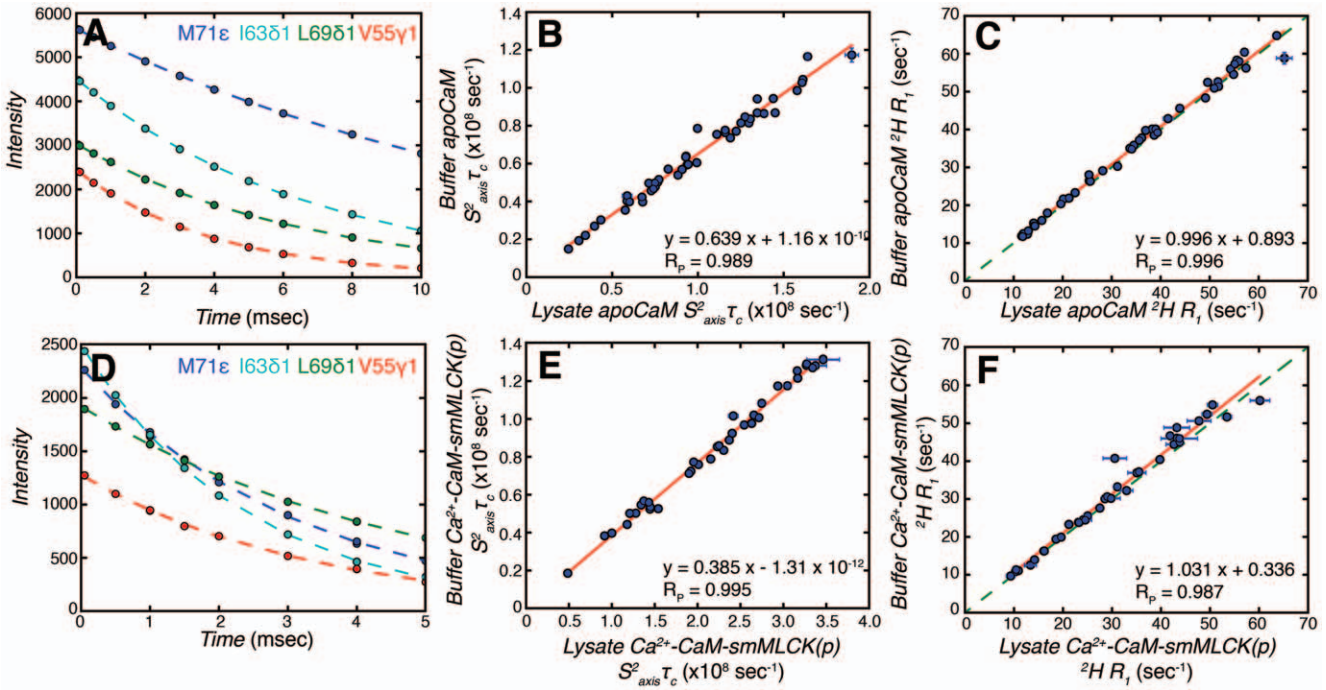

Figure 2. ^{2}H spin relaxation rates for methyl groups in lysate apoCaM and lysate Ca^{2+}-CaM-smMLCK(p). (A and D) Representative ^{2}H R_2 decay curves for (A) lysate apoCaM and (D) lysate Ca^{2+}-CaM-smMLCK(p). (B and E) Linear correlation plots of/values for methyl groups in (B) apoCaM and (E) Ca^{2+}-CaM-smMLCK(p) dissolved in either aqueous buffer (Y-axis) or lysate (X-axis). The best-fit line to the data is shown in red along with Pearson's correlation coefficient, R_p. (C and F) Linear correlation plots of ^{2}H R_1 relaxation rates measured for (C) apoCaM and (F) Ca^{2+}-CaM-smMLCK(p) in aqueous buffer (Y-axis) and lysate (X-axis). The green dashed line is y = x, while the red line is obtained from linear regression.
doi:10.1371/journal.pone.0048226.g002

Results and Discussion

Methyl Labeling Strategy and NMR Spectra

Figure 1A illustrates the methyl side-chain labeling strategy utilized in this study in which U-[^{2}H], Ile-δ1[^{13}CHD$_2$]-, Leu,Val-[^{13}CHD$_2$,^{13}CHD$_2$]-, Met[^{13}CHD$_2$]-labeled proteins were produced. This labeling scheme was chosen for several reasons. First, ^{13}C-^{1}H correlation spectra of recombinant, labeled CaM recorded in the complex, unlabeled lysate mixture could be simplified by editing through the attached deuterons, ensuring that only cross peaks from CaM are observed. Second, transverse relaxation of the deuteron is rapid (on the order of several ms in the applications considered here) and the ^{2}H gyromagnetic ratio is small so that there is negligible contribution to magnetization decay from chemical exchange [36]. We show below that this is critically important for the extraction of accurate ps-ns dynamics parameters for lysate CaM, where chemical exchange contributions to the transverse relaxation of spin ½ nuclei can be significant. Third, the ^{13}CHD$_2$ labeling scheme is well suited for recording ^{1}H CPMG relaxation dispersion profiles as a probe of ms time-scale motions [35].

Recombinant, U-[^{2}H], Ile-δ1[^{13}CHD$_2$]-, Leu,Val-[^{13}CHD$_2$, ^{13}CHD$_2$]-, Met[^{13}CHD$_2$]-labeled samples of CaM (1 mM) were over-expressed and purified from *E. coli* and then added to concentrated, unlabeled (protonated) *E. coli* lysate (final lysate protein concentration of 100 g/L). In the following study we prefer to mimic "in-cell" conditions using *E. coli* lysate rather than perform "true" *in vivo* experiments in which the protein of interest is either over-expressed in *E. coli* [15,24,26,28,29] or injected into Xenopus oocytes [19,21,23]. The use of lysate samples obviates the constant need to verify that the recorded signal derives from intracellular rather than extracellular protein, the latter due to leakage from dead or damaged cells [37]. In this regard lysate samples have proven to be stable over periods of several months and samples can be used repeatedly provided that the lysate is periodically mixed to remain homogeneous. In addition, high quality, quantitative NMR data can be recorded on lysate CaM samples since reasonable concentrations of CaM can be added; the lower CaM concentrations typical of over-expression or injection techniques and the short amounts of measurement time prior to protein leakage are significant obstacles to "in cell" NMR. Finally, lysate samples are easily manipulated by including additives in ways which are much more difficult in the case of *in vivo* experiments (see below).

Figure 1B shows Metε, Ileδ1 and Leuδ/Valγ regions from 2D ^{2}H-edited ^{13}C-^{1}H correlation spectra recorded on apoCaM, Ca^{2+}-CaM and Ca^{2+}-CaM-smMLCK(p), each in 100 g/L *E. coli* lysate. High quality correlation maps are obtained for both apoCaM and Ca^{2+}-CaM-smMLCK(p) while a noticeably poorer quality spectrum is derived from Ca^{2+}-CaM. These differences can be understood in terms of the structures of each state, as illustrated in Figure 1C. For example, in apoCaM the majority of the methyl side-chains are buried inside the hydrophobic cores of the N- and C-terminal domains [38,39], leading to high quality correlation spectra. Upon binding of four Ca^{2+} ions, large structural changes occur to CaM resulting in the exposure of many of the methyl side-chains, especially those of the nine Met residues in the protein (green spheres in Figure 1C) [40]. This rearrangement is responsible for the large chemical shift differences between corresponding peaks in the apoCaM and Ca^{2+}-CaM spectra [41]. It also leads to significant peak broadening due to transient non-specific interactions with native proteins in the lysate, as is discussed below. Upon smMLCK peptide binding, the majority of the methyl side-chains are again sequestered within the hydro-

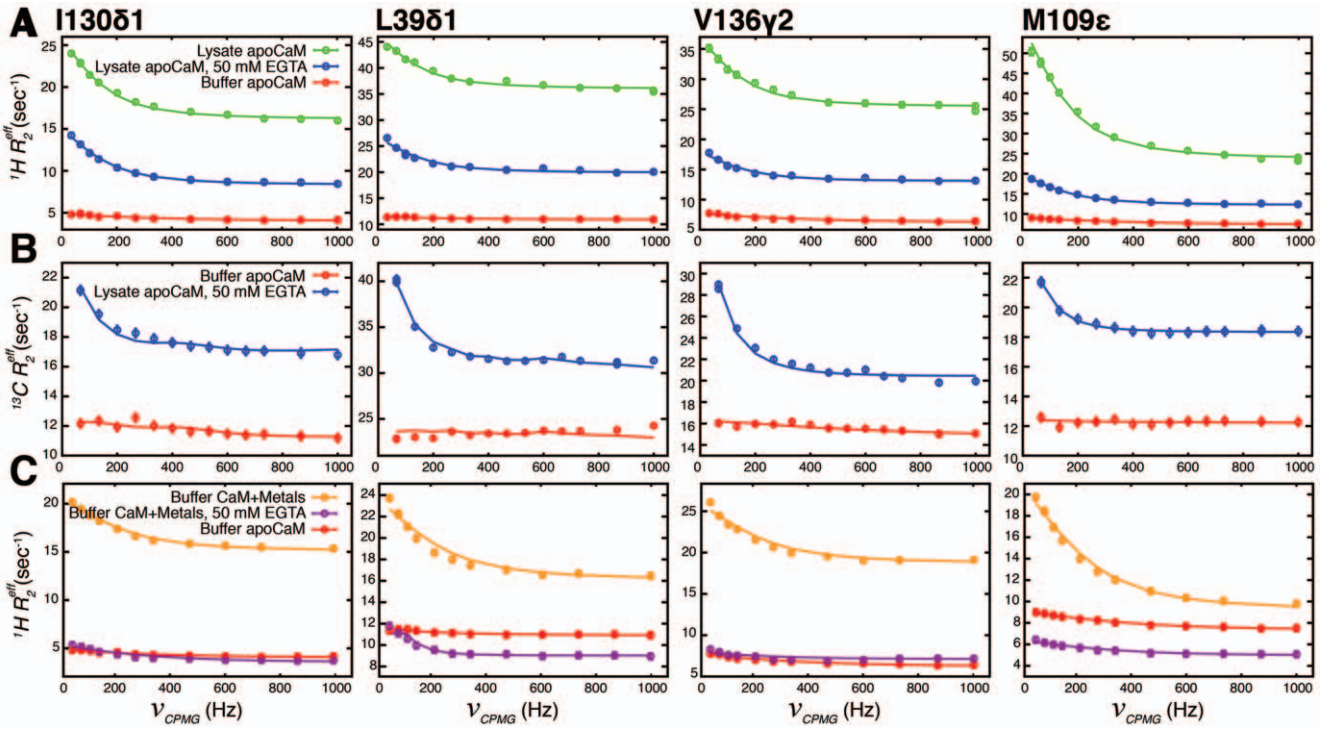

Figure 3. Chemical exchange in lysate apoCaM. Representative CPMG relaxation dispersion profiles for methyl groups I130δ1, L39δ1, V136γ2 and M109ε. (A) ^{1}H CPMG dispersion curves for lysate apoCaM (green, 100 g/L *E. coli* proteins), lysate apoCaM, 50 mM EGTA (blue) and buffer apoCaM (red). (B) ^{13}C CPMG dispersion profiles for buffer apoCaM (red) and lysate apoCaM, 50 mM EGTA (blue). (C) ^{1}H CPMG dispersion curves for buffer, CaM with (orange) or without (red) metals found in *E. coli* lysate, or with metals and 50 mM EGTA (purple). Solid lines are the result of global fits of the data to a two-site exchange model.
doi:10.1371/journal.pone.0048226.g003

phobic core of Ca^{2+}-CaM-smMLCK(p) [42] and a high quality correlation spectrum is recovered.

Fast Time-scale Methyl Side-chain Dynamics

^{2}H longitudinal, R_1, and transverse, R_2, relaxation rates [31,32] were measured for the Ile, Leu, Val and Met methyl groups of apoCaM and Ca^{2+}-CaM-smMLCK(p), both in aqueous buffer and in 100 g/L *E. coli* lysate. Corresponding data were not obtained presently for Ca^{2+}-CaM dissolved in lysate as the quality of the relaxation spectra was significantly worse (see below). Figures 2A and 2D show representative decay curves used to determine ^{2}H R_2 relaxation rates for a number of methyl groups in lysate apoCaM (Figure 2A) and lysate Ca^{2+}-CaM-smMLCK(p) (Figure 2D). Similarly high quality decay curves were obtained from R_1 measurements. Our choice of using the ^{2}H as a probe of ps-ns time-scale dynamics is based on the fact that its relaxation is dominated by the quadrupolar interaction, thus minimizing contributions from chemical exchange to transverse relaxation rates [36]. This is a particular concern for studies of CaM in lysate where we show in what follows that chemical exchange can be particularly pervasive leading to significantly elevated transverse relaxation rates for spin ½ nuclei (such as ^{1}H, ^{15}N or ^{13}C) and thus erroneous extracted dynamics parameters, unless special care is taken [43]. By contrast, ^{2}H relaxation rates are much less sensitive to such effects, as illustrated below.

As has been described in detail previously, for a $^{13}CHD_2$ group and under the conditions of our experiments, the effective ^{2}H R_2 and R_1 relaxation rates are related to motional parameters via the relations, [31,32]

$$R_2 = \frac{1}{80}(2\pi Q_{CC})^2[9J(0)+15J(\omega_D)+6J(2\omega_D)] \quad (1)$$

and

$$R_1 = \frac{3}{40}(2\pi Q_{CC})^2[4J(\omega_D)+4J(2\omega_D)]. \quad (2)$$

In its simplest form, the spectral density function, $J(\omega)$, is defined as [44,45]

$$J(\omega) = \frac{\frac{1}{9}S^2_{axis}\tau_C}{1+(\omega\tau_C)^2} + \frac{(1-\frac{1}{9}S^2_{axis})\tau}{1+(\omega\tau)^2}. \quad (3)$$

In eqs 1,2 $Q_{cc} = 167$ kHz is the ^{2}H quadrupolar coupling constant [46], $\tau^{-1} = \tau_C^{-1} + \tau_f^{-1}$, τ_C is the rotational correlation time assuming isotropic tumbling, τ_f is a time constant for ps time-scale C-D bond vector fluctuations that include methyl rotation and S^2_{axis} is the square of an order parameter that describes the amplitude of motion of the methyl rotation axis. In a "typical" analysis, values of τ_f and S^2_{axis} are extracted from fits of R_1, R_2 rates to the model described above, eqs 1–3, assuming a value for τ_C that is obtained from backbone ^{15}N spin relaxation experiments [36,47–49]. Here we have taken a different strategy that avoids complications that emerge from a potentially erroneous τ_C value

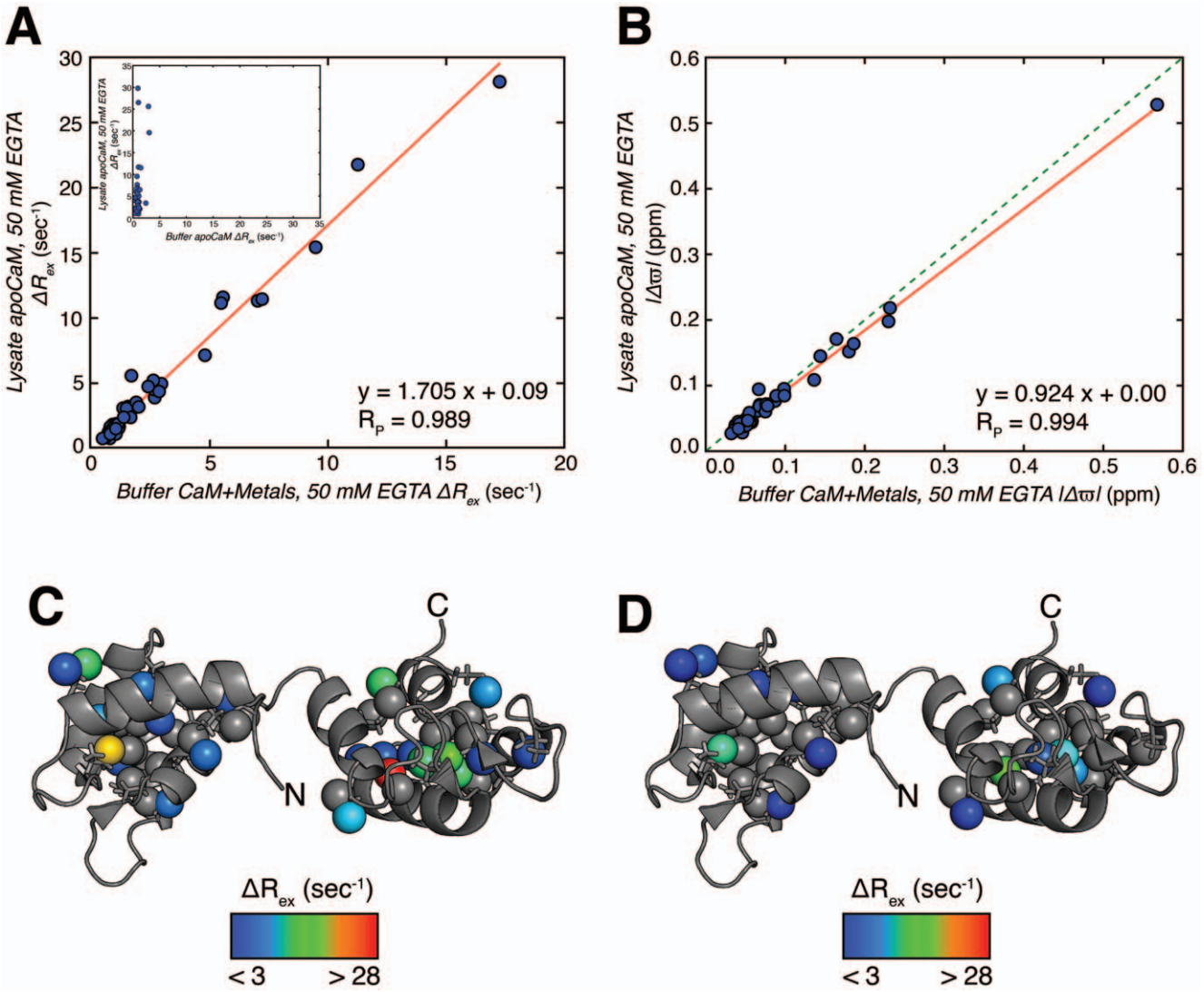

Figure 4. A major contribution to chemical exchange in lysate apoCaM from metal binding. (A) Linear correlation plot of ^{1}H ΔR_{ex} values calculated from dispersion profiles recorded on lysate apoCaM, 50 mM EGTA (Y-axis) and buffer CaM+metal, 50 mM EGTA (X-axis; metals added to approximate concentrations in *E. coli* lysate). The best-fit line is shown in red. Inset shows a poor correlation between lysate apoCaM, 50 mM EGTA (Y-axis) and buffer apoCaM (X-axis), providing further evidence that dispersions in lysate derive from metal. (B) Linear correlation plot as in (A) of $|\Delta\varpi|$ values extracted from fits of ^{1}H CPMG dispersion profiles to a model of two-site chemical exchange. (C and D) Structures of apoCaM (1DMO) [38] color coded according to methyl ^{1}H ΔR_{ex} values as measured from dispersion profiles recorded on lysate apoCaM, 50 mM EGTA (C) and buffer CaM+metal, 50 mM EGTA (D). Methyl groups with ^{1}H ΔR_{ex} <3 sec^{-1} are colored gray.
doi:10.1371/journal.pone.0048226.g004

resulting from ^{15}N relaxation rates "contaminated" by chemical exchange.

Since our goal presently is to compare ps-ns time-scale dynamics of different states of CaM in buffer or lysate we will not attempt to separate S^2_{axis} and τ_C which would require an accurate value for τ_C (assuming of course that the overall tumbling can be described by a single correlation time in the first place). Rather, from measurements of ^{2}H R_1 and R_2 rates we show below that accurate per-residue $S^2_{axis}\tau_C$ values can be isolated and can then be compared between samples to establish similarities in amplitudes of motion. Further, as described previously [31], in the macromolecular limit that is appropriate in the studies here (see below) a per-residue comparison of ^{2}H R_1 rates can be used to evaluate the similarity in τ_f values between corresponding methyl sites in different samples.

In the limit that $(\omega_D\tau_C)^2 \gg 1$, $(\omega_D\tau)^2 \ll 1$ eqs 1,2 can be rewritten as

$$R_1 = \frac{1}{80}(2\pi Q_{CC})^2\left[\frac{3.33S^2_{axis}}{\omega_D^2\tau_C} + 48\left(1-\frac{1}{9}S^2_{axis}\right)\tau\right]$$
$$R_2 = \frac{1}{80}(2\pi Q_{CC})^2\left[S^2_{axis}\tau_C + \frac{11S^2_{axis}}{6\omega_D^2\tau_C} + 30\left(1-\frac{1}{9}S^2_{axis}\right)\tau\right] \quad (4)$$

and the errors introduced by these simplifying assumptions are small. For example, for $\tau_C = 4$ ns, $S^2_{axis} = 0.5$, $\tau_f = 20$ psec, 14.0T errors of 8.6 and 3.3% are obtained for the R_1, R_2 rates, respectively, that decrease to 0.33 and 0.02% for $\tau_C = 15$ ns. As S^2_{axis} increases the errors become slightly larger ($\tau_C = 4$ ns, $S^2_{axis} = 1.0$, $\tau_f = 20$ psec, 14.0 T, errors of 11 and 3.5%; $\tau_C = 15$ ns,

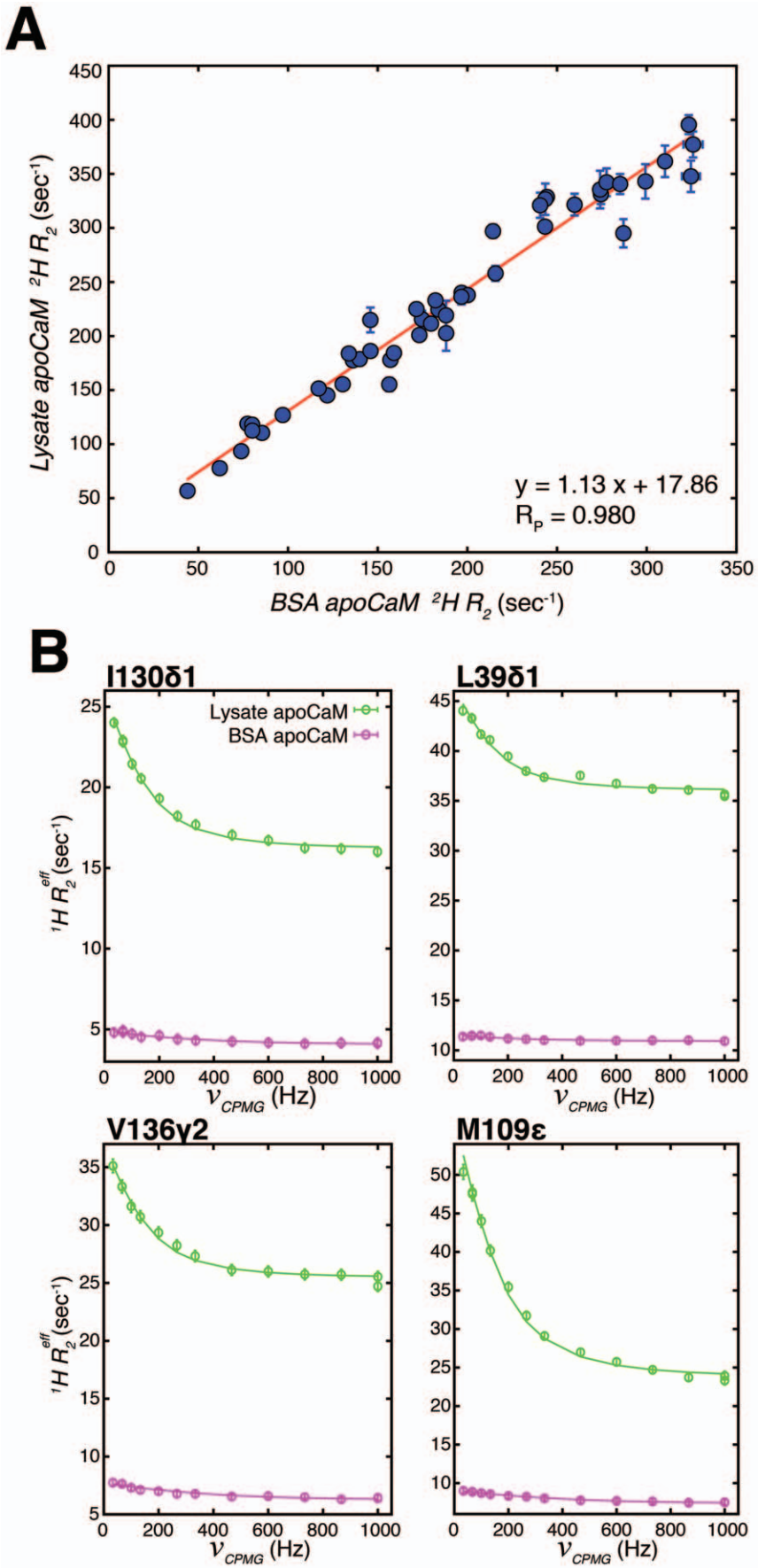
A
Lysate apoCaM ^2H R_2 (sec^{-1})
BSA apoCaM ^2H R_2 (sec^{-1})
y = 1.13 x + 17.86
R_P = 0.980
B
I130δ1
L39δ1
V136γ2
M109ε
Lysate apoCaM
BSA apoCaM
^1H R_2^{eff} (sec^{-1})
ν_{CPMG} (Hz)

Figure 5. Chemical exchange in lysate apoCaM is not due to crowding. (A) Linear correlation plot of methyl ^{2}H R_2 relaxation rates from lysate apoCaM (Y-axis) and BSA apoCaM (200 g/L BSA, X-axis). Best-fit line in red. (B) Representative ^{1}H CPMG relaxation dispersion profiles for BSA apoCaM (pink) and lysate apoCaM (green). The solid lines derive from global fits of dispersion profiles to a two-site exchange model.
doi:10.1371/journal.pone.0048226.g005

$S^2_{axis}=1.0$, $\tau_f=20$ psec, errors of 0.5 and 0.03%), but are still negligible for applications involving the size of proteins considered here (see below). Similarly small errors are obtained over the range of τ_f values typically observed (10 ps $\leq \tau_f \leq$100 ps). Combining expressions for R_1 and R_2 above one obtains

$$R_2=\frac{1}{80}(2\pi Q_{CC})^2[S^2_{axis}\tau_C+\frac{50R_1}{(2\pi Q_{CC})^2}-\frac{0.25S^2_{axis}}{\omega_D^2\tau_C}]. \quad (5)$$

It is straightforward to show that the final term in eq 5 is small and can be neglected for any reasonable values of dynamics parameters. For $\tau_C=2$ ns, $S^2_{axis}=0.5$, $\tau_f=20$ psec, 14.0 T, omission of this term introduces an error of $\sim$ 8.0% that decreases to 0.1% for $\tau_C=20$ ns. In general, errors increase very slightly as a function of S^2_{axis} and for decreasing values of τ_f and decrease with increasing τ_C but do not exceed 10% even for $\tau_C=2$ ns.

Tjandra *et al* have analyzed ^{15}N backbone relaxation experiments recorded on apoCaM in aqueous buffer [50] and Lee *et al* have carried out similar analyses for Ca^{2+}-CaM-smMLCK(p) [51]. Taking into account the differences in temperatures between their work and that reported here, as well as the different solvent systems used (100%D_2O *vs.* 90%H_2O, 10%D_2O), the N- and C-terminal domains of apoCaM are predicted to tumble with correlation times of $\sim$17 and $\sim$14 nsec, respectively, under our conditions (18°C), while both domains of Ca^{2+}-CaM-smMLCK have predicted τ_C values of $\sim$15 nsec. Correlation times will, of course, be higher in lysate (see below). The final term in eq 5 contributes no more than 0.3% to R_2 and can therefore be neglected in our work here. Thus, from measurement of both R_2 and R_1 values it is possible to obtain accurate values of the product $S^2_{axis}\tau_C$.

Figure 2B shows the linear correlation plot of $S^2_{axis}\tau_C$ values for methyl groups of apoCaM in buffer (Y-axis, buffer apoCaM) and in 100 g/L *E coli* lysate (X-axis, lysate apoCaM) with the corresponding plot for Ca^{2+}-CaM-smMLCK(p) indicated in panel E. An excellent correlation is obtained for both datasets, with Pearson's correlation coefficients of 0.989 and 0.995, respectively, indicating that for both states of CaM S^2_{axis} values are the same in lysate and aqueous buffer. Moreover, the excellent correlations observed in Figures 2B,E also establish that the methodology outlined above for extracting values of $S^2_{axis}\tau_C$ is robust, as expected based on anticipated errors described above. Not surprisingly there is an increase in τ_C for samples dissolved in lysate relative to buffer that manifests in a slope different from unity. Despite the fact that very similar concentrations of lysate are used for apoCaM and Ca^{2+}-CaM-smMLCK(p) samples, the relative increase in tumbling time is significantly more for peptide bound CaM (lysate *vs* buffer), reflecting the differences in shapes of the two molecules.

Figures 2C and 2F plot ^{2}H R_1 values for methyl groups of CaM dissolved in buffer and lysate and a very high degree of correlation is obtained. Simulations establish that for τ_C values on the order of 15 and 30 ns, as is the case for CaM dissolved in buffer and lysate, respectively, an agreement between R_1 rates of the sort illustrated here with a slope of 1 is only possible if the τ_f values for a given methyl group are very similar for both buffer and lysate solvents.

In summary, the results presented above establish that, at least in the context of a simple model of protein ps-ns time-scale dynamics and for apoCaM and Ca^{2+}-CaM-smMLCK(p) samples, motional parameters (in this case S^2_{axis}, τ_f) are unaffected by lysate. Previous studies have indicated that protein dynamics may be slaved to solvent motion and that perturbations to solvent can be 'felt' within the protein hydrophobic core [52–56]. In this context our results suggest that the properties of the solvent surrounding CaM in lysate and aqueous buffer are similar – at least with regard to coupling to fast time-scale protein dynamics - consistent with ^{2}H R_2 measurements of D_2O in living bacterial cells performed by Persson and Halle, where it was determined that $\sim$85% of cell water has bulk-like dynamics [57].

Chemical Exchange in Lysate apoCaM

Results described in the previous section indicate that ps-ns time-scale side-chain dynamics of methyl containing residues in apoCaM and Ca^{2+}-CaM-smMLCK(p) are very similar. In an effort to extend our study to additional time-scales we have recorded ^{1}H- and to a lesser extent ^{13}C-CPMG [35,58] relaxation dispersion experiments that probe ms motions. As described above, the methyl side chains of apoCaM are predominantly buried within the hydrophobic cores of the N- and C-terminal domains [38,39] and are thus unavailable for interaction with the natural proteins of the *E. coli* lysate. Our initial assumption was, therefore, that there would be little difference between buffer and lysate apoCaM with respect to slow timescale dynamics, as probed by methyl groups. Representative ^{1}H CPMG dispersion profiles, Figure 3A, illustrated for 4 residues of apoCaM show that this is, indeed, not the case. For many of the methyl groups in the protein significant dispersion profiles were measured for lysate apoCaM (green circles), indicating ms timescale conformational exchange. Excellent fits (solid lines) of methyl dispersion data recorded at 14.0 T were obtained using a two-site chemical exchange model [59], with a global exchange rate of 880 ± 30 s^{-1} between interconverting conformations (see Materials and Methods). By contrast, the corresponding curves for buffer apoCaM (red) showed little dependence on the time between successive pulses of the CPMG element, δ, ($\nu_{CPMG}=1/(2\delta)$) and therefore much less evidence for the same ms exchange process (compare red and green curves).

In order to establish the origin of the exchange in the lysate environment we added 50 mM EGTA to the lysate apoCaM sample and repeated the ^{1}H CPMG experiments (blue). Dispersion profiles were significantly attenuated but nevertheless were not quenched, Figure 3A (compare green and blue). These results are not artifactual. ^{13}C CPMG dispersion profiles, recorded on U-[^{2}H], Ile-δ1[$^{13}CH_3$]-, Leu, Val-[$^{13}CH_3$, $^{12}CD_3$]-, Met[$^{13}CH_3$]-labeled samples of apoCaM in buffer and lysate containing EGTA (Figure 3B), were similar to those recorded with the ^{1}H experiments. The partial attenuation of exchange effects upon addition of chelator provides strong evidence that metal binding to apoCaM contributes at least somewhat to the CPMG dispersion profiles. To investigate this more fully we have prepared a sample of buffer apoCaM to which has been added metals in concentrations corresponding to those found in *E. coli* lysate (free + bound metal), as determined by atomic absorption analysis (see Materials and Methods). No attempt has been made to compensate for the fact that some of the metals will be sequestered by proteins in the

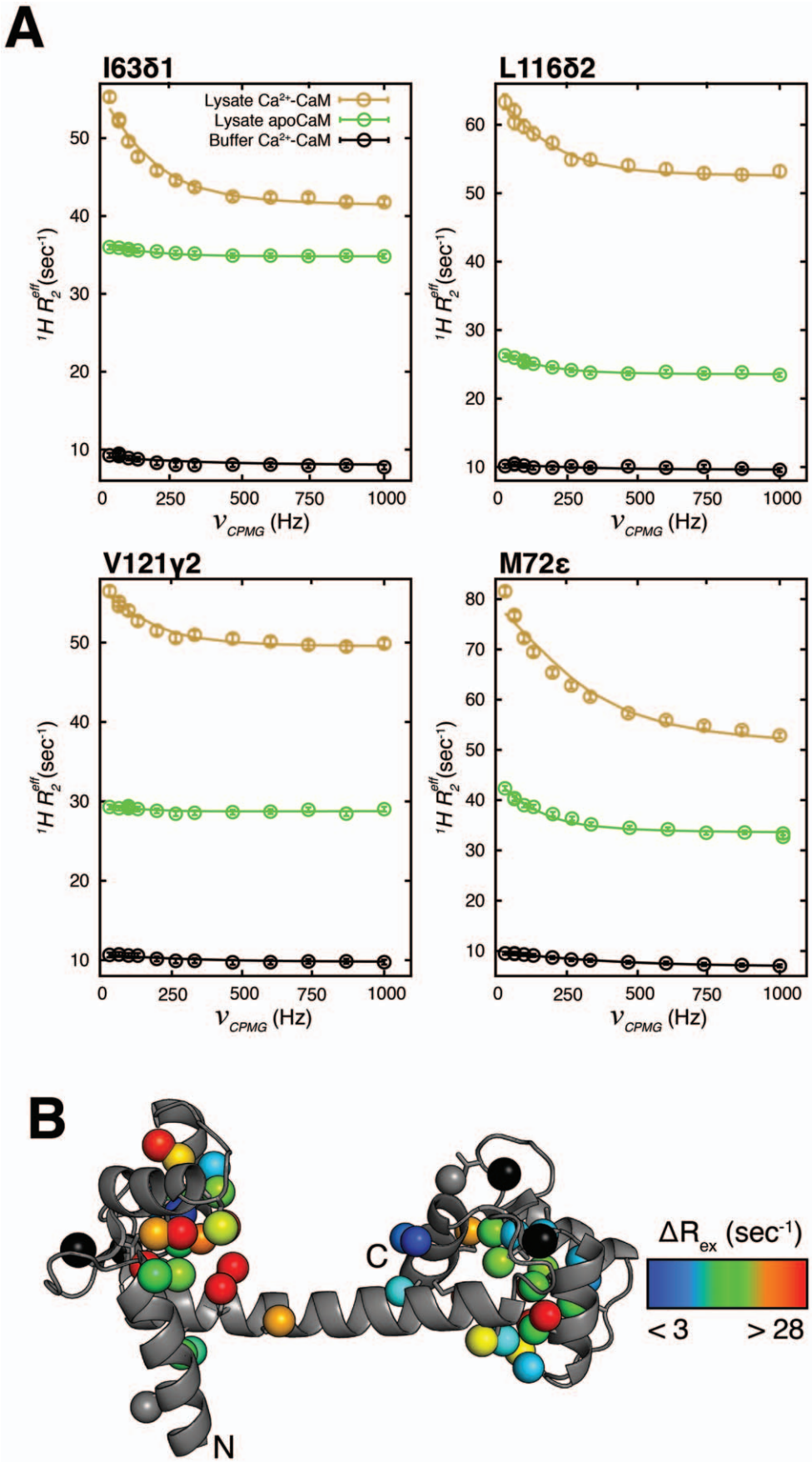
A
I63δ1
L116δ2
V121γ2
M72ε
Lysate Ca2+-CaM
Lysate apoCaM
Buffer Ca2+-CaM
1H R2eff(sec-1)
νCPMG (Hz)
B
C
N
ΔRex (sec-1)
< 3
> 28

Figure 6. Pervasive chemical exchange in lysate Ca^{2+}-CaM. (A) Representative ^{1}H CPMG relaxation dispersion profiles from I63δ1, L116δ2, V121γ1 and M72ε methyl groups of buffer Ca^{2+}-CaM (black) and lysate Ca^{2+}-CaM, 6 mM Ca^{2+} (brown). For comparison, dispersion curves are also shown for lysate apoCaM (green). (B) Structure of Ca^{2+}-CaM (3CLN) [40] with methyl groups color coded according to ^{1}H ΔR_{ex} values. Methyl groups with ^{1}H ΔR_{ex} <3 sec^{-1} are colored gray. The four Ca^{2+} ions are shown as black spheres.
doi:10.1371/journal.pone.0048226.g006

lysate, as the fraction bound is unknown. Large dispersion profiles are observed, Figure 3C (orange) that are of a similar magnitude to those recorded for the lysate, apoCaM sample (Figure 3A, green). These dispersions can be attenuated significantly, but not eliminated, by addition of 50 mM EGTA, Figure 3C purple, as observed upon addition of chelator to lysate, apoCaM (Figure 3A, blue).

The effect of metal can be quantified more fully by comparing the magnitudes of ^{1}H dispersion profiles, $\Delta R_{ex} = R_2^{eff}(\nu_{CPMG}^{MAX}) - R_2^{eff}(\nu_{CPMG}^{MIN})$, recorded on samples of lysate apoCaM, EGTA and buffer CaM+metal, EGTA. Figure 4A shows an excellent correlation between ΔR_{ex} values, consistent with similar exchange processes in both cases. By contrast, a poor correlation is obtained when values from samples of lysate apoCaM, EGTA and buffer apoCaM (*i.e.*, no added metal) are compared (Figure 4A, inset) that provides further evidence that the dispersions observed in the lysate derive largely from metal exchange (see below). Dispersion profiles for lysate apoCaM, EGTA and buffer CaM+metal, EGTA have been fitted to a model of two-site exchange and extracted absolute values of chemical shift differences, $|\Delta\varpi|$ (ppm), are in good agreement, Figure 4B, as would be expected for exchange processes sharing a common mechanism. Fitted values of k_{ex} are similar between samples, but not identical ($k_{ex}^{Lysate} = 600 \pm 55\ s^{-1}$, $k_{ex}^{Buffer} = 750 \pm 90\ s^{-1}$), reflecting potential differences in metal concentrations as well as differences in on/off rates between crowded lysate and buffer environments. The fitted values of $|\Delta\varpi|$ and k_{ex} also rationalize the linear relationship of Figure 4A, where for the majority of residues $k_{ex}^2 > \Delta\omega^2$. In this limit it can be shown [60] that a plot of *vs* ΔR_{ex}^{Buffer} would be expected to be approximately linear assuming that a two-site exchange mechanism is valid (*i.e.*, binding occurs to predominantly a single, high affinity site) with $\Delta R_{ex}^{Lysate} \approx \frac{(p_F p_B/k_{ex})^{Lysate}}{(p_F p_B/k_{ex})^{Buffer}} \Delta R_{ex}^{Buffer}$, where p_F and $p_B = 1 - p_F$ are the fractional populations of metal free and metal bound states. Note that while an excellent correlation of ΔR_{ex} values is predicted in this case, the slope of the correlation plot $(\frac{(p_F p_B/k_{ex})^{Lysate}}{(p_F p_B/k_{ex})^{Buffer}})$ can differ from unity. From the fitted exchange parameters ΔR_{ex}^{Lysate} is calculated to be greater than ΔR_{ex}^{Buffer}, as observed (Figures 3A,C and 4A), that is not inconsistent with metal exchange playing a major role in the exchange process in both cases.

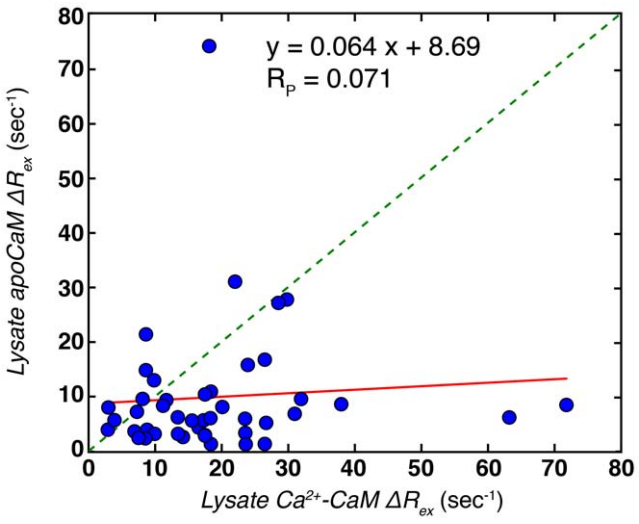

Figure 7. Slow time-scale dynamics in lysate Ca^{2+}-CaM do not derive from metal binding. Linear correlation plot of ^{1}H ΔR_{ex} values from lysate apoCaM (Y-axis) and lysate Ca^{2+}-CaM with 6 mM Ca^{2+} (X-axis). The red line derives from linear regression of the data.
doi:10.1371/journal.pone.0048226.g007

Figures 4C, D show that the large ΔR_{ex} values from lysate and buffer+metal CaM samples (with EGTA) localize to the same sets of residues. Most of the methyl groups with substantial ΔR_{ex} can be found in the C-terminal domain and include V108Cγ1, V91Cγ1, I100Cδ1 and L105δ1/δ2, located in Ca^{2+}-binding site-III, which has the highest affinity for Ca^{2+} [61]. It has previously been demonstrated that site-III is the first to bind Ca^{2+}, [61] so that at sub-stoichiometric Ca^{2+} concentrations (recall that 50 mM EGTA has been added) exchange between free and bound conformers would be expected in this region.

These results clearly establish that metal exchange in lysate apoCaM plays a very significant role in the ms dynamics that are observed and that contributions from interactions with endogenous *E. coli* proteins in lysate are at most only very minor. Indeed, the correlations observed in Figures 4A,B would not be obtained otherwise. As an aside it appears that 50 mM EGTA is not sufficient to sequester all of the metal and quench the exchange process. We were interested to see if there is an additional component to the dispersions that might derive from macromolecular crowding. To this end we prepared a sample of apoCaM in buffer containing 200 g/L BSA (referred to as a BSA apoCaM sample). This concentration of BSA results in a similar macroscopic viscosity to that obtained with 100 g/L lysate, as established by a comparison of ^{2}H R_2 values for CaM measured in lysate and BSA samples, Figure 5A. In the macromolecular limit $R_2 \propto S_{axis}^2 \tau_C$, eq 5, and the similar R_2 values obtained in the two samples imply, therefore, comparable CaM tumbling times and hence similar solution viscosities. Figure 5B compares ^{1}H CPMG dispersion profiles of lysate apoCaM and BSA apoCaM samples. Profiles from BSA apoCaM are very much smaller than for lysate apoCaM so that if crowding does in fact contribute to ms dynamics it does so only in a very minor way.

Interestingly, fluorescence experiments on and computer simulations of apoCaM in the crowded environment of the inert glucose polymer Ficoll indicate that crowding (i) lowers the inter-domain distance (see Figure 1C) producing a second population of more compact structures, (ii) increases the flexibility of the C-terminal domain by weakening tertiary interactions and (iii) partially exposes hydrophobic patches responsible for substrate binding [62,63]. ^{13}C-^{1}H correlation spectra of apoCaM in both lysate and BSA are very similar to those recorded in aqueous buffer, suggesting little conformational change or alternatively one that involves only a very small population of molecules that is below the detection threshold of our experiments. Moreover, we see no differences in ps-ns internal dynamics or in ms time-scale dynamics between CaM samples in buffer or 200 g/L BSA, suggesting that if there is a change in flexibility it involves

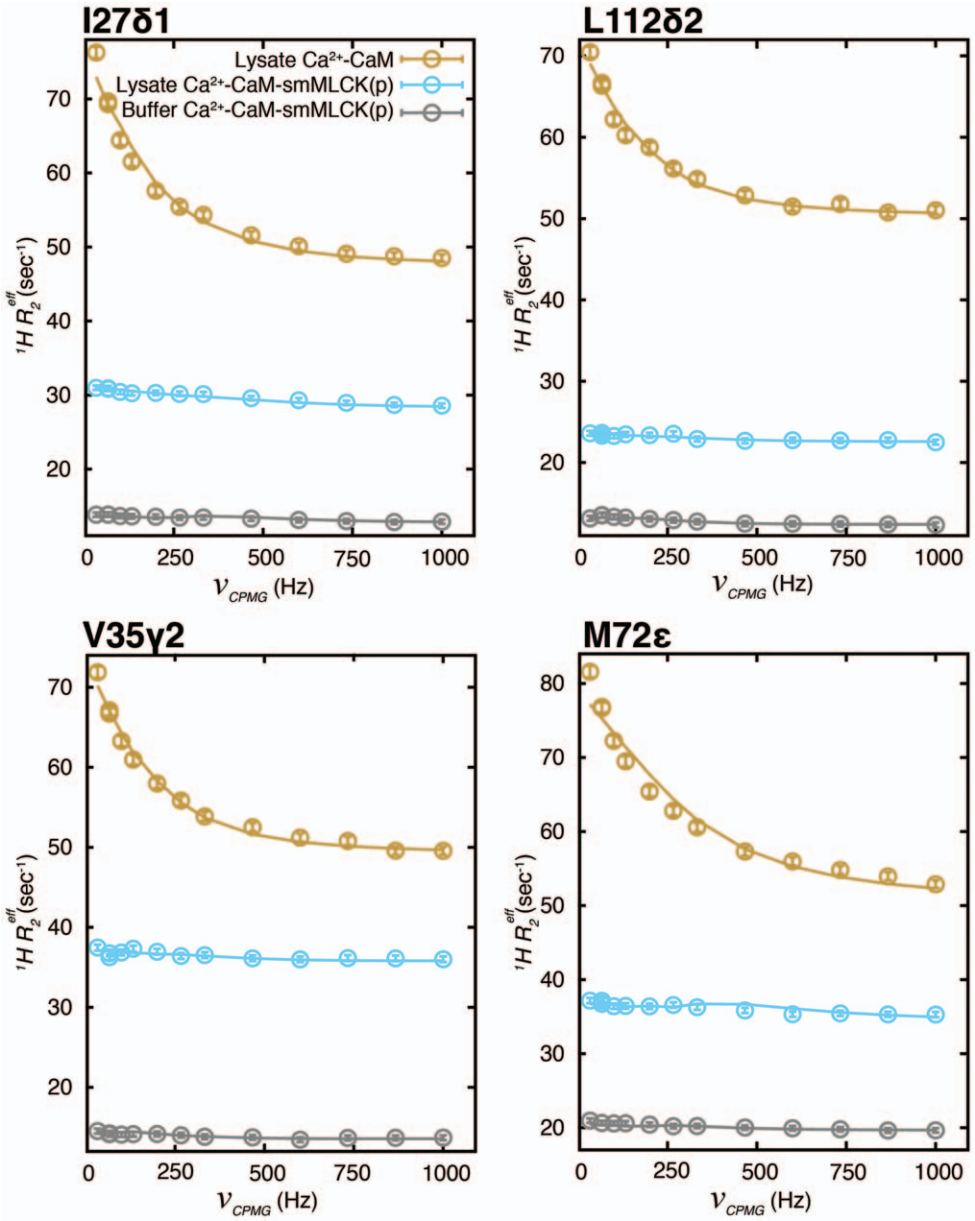

Figure 8. Chemical exchange in lysate Ca^{2+}-CaM is eliminated through the addition of smMLCK(p). Representative ^1H CPMG relaxation dispersion curves for methyl groups I27δ1, L112δ2, V35γ2 and M72ε of lysate Ca^{2+}-CaM (brown), lysate Ca^{2+}-CaM-smMLCK(p) (light blue) and buffer Ca^{2+}-CaM-smMLCK(p) (grey). Solid lines derive from fits of profiles to a two-site global exchange model.
doi:10.1371/journal.pone.0048226.g008

frequencies that are distinct from those monitored in the present set of experiments or that the changes do not involve methyl containing residues.

Finally, Figure 5A illustrates an important point, emphasized earlier in the text, concerning the use of deuterium spin relaxation. Despite the fact that there are significant exchange contributions to ^{13}C and ^1H linewidths in spectra of apoCaM in lystate, as established by relaxation dispersion experiments (see Figure 3), these impact negligibly on ^2H R_2 rates so that accurate values are obtained. Note that the excellent correlation in Figure 5A could not be realized if the ms dynamics in the lysate apoCaM sample were to significantly influence ^2H R_2 rates. In this context we have found that ^{13}C transverse relaxation rates of methyl groups in lysate apoCaM (measured using $^{13}CHD_2$ probes) are consistently larger than expected based on ^2H measurements. As discussed previously, the deuteron is an excellent probe precisely because its relaxation is dominated by the well-understood quadrupolar mechanism [36,64].

Extensive ms Time-scale Motions in Lysate Ca^{2+}-CaM but not in Lysate Ca^{2+}-CaM-smMLCK(p)

The ligation of Ca^{2+} to the four metal binding sites in CaM is accompanied by significant conformational changes. These involve the majority of the methyl groups in the molecule that are displaced from the hydrophobic cores of the N- and C-terminal domains, relocalizing to surface exposed positions primed for binding target proteins [40]. Interestingly, ^1H CPMG relaxation dispersion profiles of lysate Ca^{2+}-CaM (10% trimmed

mean $\Delta R_{ex} = 17.0\ s^{-1}$) are significantly larger than for lysate apoCaM (10% trimmed mean $\Delta R_{ex} = 8.5\ s^{-1}$), as illustrated for a number of residues in Figure 6A (compare brown *vs* green). The exchange process is wide-spread, affecting all but 2 of the methyl groups in CaM, Figure 6B, while by comparison, ms time-scale dynamics in lysate apoCaM are mostly confined to the C-terminal domain. Additionally, $k_{ex} = 1250 \pm 30\ s^{-1}$, from fits of lysate Ca^{2+}-CaM dispersion profiles is double that determined for lysate apoCaM ($600 \pm 55\ s^{-1}$). It is clear, therefore, that the exchange dynamics are very different between lysate apoCaM and lysate Ca^{2+}-CaM; indeed this must be the case as metal exchange is much less prevalent in the Ca^{2+} loaded form of the protein (in the presence of excess Ca^{2+}), while it is the major source of the broadening in lysate apoCaM. That the processes responsible for conformational heterogeneity in the two CaM states are very different is further shown in Figure 7 where ΔR_{ex} values for lysate apoCaM and lysate Ca^{2+}-CaM are poorly correlated. Finally, it is noteworthy that Akke and coworkers have measured much faster dynamics in a Ca^{2+} loaded-CaM C-terminal domain mutant using ^{15}N $R_{1\rho}$ type of experiments ($k_{ex} \sim 20$ μs) that are linked to a transition between open and closed conformational states related to metal release [65].

The exposure of hydrophobic methyl containing side-chains upon addition of Ca^{2+} to CaM and the availability of a large number of native *E. coli* proteins in lysate that can potentially serve as weak, non-specific targets for Ca^{2+}-CaM suggests that the pervasive ms fluctuations may derive from weak binding events. Indeed, Met side-chains play a pivotal role in substrate recognition [42,51] and all of the Metε groups show exchange, with the largest ΔR_{ex} values obtained for M124ε ($72\ s^{-1}$) and M71ε ($63\ s^{-1}$), respectively. If the exchange derives from a "frustrated" search process whereby Ca^{2+}-CaM interacts with a range of non-cognate *E. coli* proteins then the ms dynamics is predicted to be quenched by addition of a high affinity target peptide, such as from the protein smooth muscle myosin light chain kinase (smMLCK). Peptide binding would sequester the hydrophobic methyl containing side-chains in a single conformation and hence eliminate exchange. Addition of smMLCK peptide ($K_d = 1$ nM [51]) leads to a markedly improved ^{13}C-^{1}H correlation map (compare lysate Ca^{2+}-CaM and lysate Ca^{2+}-CaM-smMLCK(p), Figure 1B) and essentially eliminates ms timescale motions as detected via ^{1}H CPMG relaxation dispersion experiments, Figure 8.

Concluding Remarks

It is well known that the cellular milieu is very distinct from the highly controlled environment that is typically employed in "test-tube" studies of protein molecules. The large number of diverse biomolecules in the cell, including proteins, nucleic acids, lipids and metabolites and the high net concentration of protein molecules that typically greatly exceeds that used in *in vitro* biophysical studies can potentially lead to changes in protein structure and dynamics. Here we have presented a comparative study of methyl containing side-chain dynamics of CaM in apo, Ca^{2+}-loaded and Ca^{2+}-loaded peptide bound states dissolved in either buffer or *E. coli* lysate. Very similar ^{13}C-^{1}H methyl correlation spectra are obtained for apoCaM and Ca^{2+}-CaM-smMLCK(p) in buffer and lysate indicating that the average structures of these states do not change with the different protein environments. By contrast, significant differences are observed in spectra of buffer and lysate Ca^{2+}-CaM both in terms of linewidths and peak positions (Figure 1B) that likely reflect non-specific transient interactions between CaM and non-cognate protein partners in *E. coli* lysate. ^{2}H spin relaxation experiments establish that ps-ns dynamics for apoCaM and Ca^{2+}-CaM-smMLCK(p) are little affected by lysate, while the significant ms processes measured for lysate apoCaM and lysate Ca^{2+}-CaM are absent in aqueous buffer. This study emphasizes both the similarities and the differences in protein dynamics between aqueous and in-cell like conditions and serves as a reminder that a complete understanding of protein structure and dynamics must ultimately take into account the unique cellular environment in which the protein functions.

Materials and Methods

Sample Preparation

BL21(DE3) pLysS *E. coli* cells (EMD Millipore) were transformed with a plasmid encoding CaM and were grown in deuterated M9 minimal media with 1 g/L $^{15}NH_4Cl$ and 3 g/L $^{2}H,^{12}C$-glucose at 37°C. Production of U-[^{2}H],Ile-δ1[$^{13}CHD_2$]-, Leu,Val-[$^{13}CHD_2$,$^{13}CHD_2$]-, Met[$^{13}CHD_2$]-labeled samples of CaM followed the protocol of Tugarinov *et al* with precursors added to the bacterial culture 1 hour before induction [66]. Over-expression of CaM was induced with 1 mM IPTG and proceeded overnight at 30°C. The resulting His-tagged protein was purified on a HisTrap HP column (GE Healthcare), followed by TEV protease cleavage of the His-tag and repurification over HisTrap HP and HiTrap Phenyl HIC HP columns (GE Healthcare). Purified CaM was buffer exchanged into the appropriate NMR buffer and concentrated using a 3 kDa MWCO centrifugal concentrator (Amicon). For apoCaM, the NMR buffer was 20 mM imidazole, pH 6.5 (uncorrected), 100 mM KCl, 1.5 mM EGTA, 100 μM NaN_3 in 100% D_2O. For Ca^{2+}-CaM and Ca^{2+}-CaM-smMLCK(p) samples, the buffer was 20 mM imidazole, pH 6.5 (uncorrected), 100 mM KCl, 6 mM $CaCl_2$, 100 μM NaN_3 in 100% D_2O.

A smMLCK(p) peptide (NH_2-ARRKWQKTGHAV-RAIGRLSS-COOH) was purchased from GenScript (Piscataway, NJ) at >98% purity and was used without further purification. The peptide was resuspended in Ca^{2+}-CaM NMR buffer. Dilute solutions of peptide and Ca^{2+}-CaM were combined in a 1.25:1 molar ratio and concentrated in a 3 kDa MWCO centrifugal concentrator to produce samples of Ca^{2+}-CaM-smMLCK(p).

E. coli lysate was prepared by growing BL21(DE3) pLysS cells (EMD Millipore) in LB supplemented with chloramphenicol (34 μg/mL) at 37°C until $OD_{600} \sim 0.9$. The cells were harvested, resuspended in D_2O, lysed and the insoluble material spun down. 5 mM benzamidine, 0.1 mg/mL PMSF and 100 μM NaN_3 were added to the clarified lysate, which was then filtered through a 0.22 μm syringe filter. Subsequently lysate was concentrated in a 3 kDa MWCO centrifugal concentrator. Total lysate protein concentration was determined by the BCA assay (Pierce) and samples of CaM in lysate were produced by diluting concentrated CaM and concentrated lysate to the appropriate volumes. All NMR samples were 1 mM CaM and lysate samples contained 100 g/L *E. coli* protein. Ca^{2+}-CaM and Ca^{2+}-CaM-smMLCK(p) lysate samples were supplemented with 6 mM $CaCl_2$. The choice of 100 g/L *E. coli* protein represents a compromise between a 'physiological' amount of added protein (in cell protein concentrations range between 80 and 400 g/L) [67–69] and the ability to record very high quality spectra so that accurate relaxation data could be obtained. We estimate that reasonable quality data could be generated for lysate protein concentrations up to approximately 200 g/L.

Atomic absorption analysis was performed by the ANALEST facility of the Department of Chemistry at the University of Toronto on a 10 mg/mL sample of lysate. After correction for

dilution, the following total metal concentrations were obtained: Ba, 0.004 mM; Ca, 0.292 mM; Cu, 0.001 mM; Fe, 0.292 mM; K, 31.203 mM; Mg, 1.300 mM; Mn, 0.035 mM; Na, 29.622 mM; Ni, 0.018 mM; and Zn, 0.093 mM. A 2× solution of these metals (excluding Ba and Cu) was prepared in D_2O and mixed 1:1 with apoCaM in D_2O. EGTA was then added to 50 mM.

NMR Spectroscopy

NMR spectra were recorded at 18°C on a Varian Inova spectrometer, 14.0T, equipped with a cryogenically cooled pulsed-field gradient triple resonance probe. Data sets were typically obtained with 72x512 complex points, acquisition times of 26x64 msec in t_1 and t_2, respectively, and a 2.0 sec recycle delay. ^{2}H R_1 and R_2 relaxation rates were measured using pulse schemes described previously [31,32]. R_1 values were generated from 8 parametrically varied time points between 0.05 and 25 msec, while ^{2}H R_2 rates were based on measurements of 8 to 11 time points between 0.05 and 15 msec for samples in aqueous buffer and 0.05 and 10 ms for samples in lysate. Total measuring times were approximately 36 and 20 hours for R_1 and R_2 data sets, respectively. ^{2}H relaxation rates were subsequently obtained from fits to a single-exponential decay function, Ae^{-Rt}, with errors calculated from the covariance matrix method [70]. ^{1}H relaxation dispersion profiles were recorded using a pulse scheme described by Baldwin *et al.*, [35] with a 30 msec constant-time CPMG relaxation delay and CPMG frequencies ranging between 33.3 and 2,000 Hz (18 or 32 hours for a data set comprising 18 2D spectra recorded on samples in buffer and lysate, respectively). All spectra were processed with NMRPipe/NMRDraw software [71] and peak intensities quantified with the program FuDA (http://pound.med.utoronto.ca/software.html) [70]. ^{1}H relaxation dispersion profiles were calculated from the relation $R_2^{eff}(\nu_{CPMG}) = \frac{-1}{T}\ln\left(\frac{I(\nu_{CPMG})}{I_o}\right)$, where T is the constant-time relaxation delay, $\nu_{CPMG} = 1/(2\delta)$ with δ the delay between successive refocusing pulses in the CPMG element and $I(\nu_{CPMG})$ and I_o are peak intensities from spectra recorded with and without the delay T, respectively. Dispersion data were fitted using the program CATIA (http://pound.med.utoronto.ca/software.html) assuming a two-site global exchange model, as described previously [59,72]. Initially methyl groups with $\Delta R_{ex} > 10$ s^{-1} were fitted together to obtain global values for k_{ex} and p_B. The global parameters were then fixed and all residues were subsequently fitted together to the two-site exchange model. A number of very small dispersion profiles (less than 3–4 s^{-1}) were observed in buffer CaM (from L105Cδ1/δ2, V91Cγ1 and Val55Cγ1) that are associated with an exchange process that is unrelated to the effects of lysate. These were removed prior to fitting.

Acknowledgments

The authors thank Professor Mistu Ikura (Ontario Cancer Institute) for the gift of a CaM plasmid and for assignments of apoCaM and Ca^{2+}-CaM and Professor Josh Wand (University of Pennsylvannia) for assignments of Ca^{2+}-CaM-smMLCK(p). Dr. John Rubinstein is thanked for providing laboratory space. L.E.K. hold a Canada Research Chair in Biochemistry.

Author Contributions

Conceived and designed the experiments: MPL LEK. Performed the experiments: MPL. Analyzed the data: MPL LEK. Contributed reagents/materials/analysis tools: MPL LEK. Wrote the paper: MPL LEK.

References

1. Daniel RM, Dunn RV, Finney JL, Smith JC (2003) The role of dynamics in enzyme activity. Annu Rev Biophys Biomol Struct 32: 69–92. Available: http://www.ncbi.nlm.nih.gov/pubmed/12471064.
2. Ma B, Nussinov R (2010) Enzyme dynamics point to stepwise conformational selection in catalysis. Curr Opin Chem Biol 14: 652–659. Available: http://www.ncbi.nlm.nih.gov/pubmed/20822947.
3. Benkovic SJ, Hammes-Schiffer S (2003) A perspective on enzyme catalysis. Science 301: 1196–1202. Available: http://www.ncbi.nlm.nih.gov/pubmed/12947189.
4. Villali J, Kern D (2010) Choreographing an enzyme's dance. Curr Opin Chem Biol 14: 1–8. Available: http://www.ncbi.nlm.nih.gov/pubmed/20822946.
5. Hammes GG (2002) Multiple Conformational Changes in Enzyme Catalysis. Biochemistry 41: 8221–8228. Available: http://pubs.acs.org/doi/abs/10.1021/bi0260839.
6. Bennett BD, Kimball EH, Gao M, Osterhout R, Van Dien SJ, et al. (2009) Absolute metabolite concentrations and implied enzyme active site occupancy in Escherichia coli. Nat Chem Biol 5: 593–599. Available: http://www.pubmedcentral.nih.gov/articlerender.fcgi?artid = 2754216&tool = pmcentrez&rendertype = abstract.
7. Neidhardt FC (1987) Escherichia coli and Salmonella typhimurium. Neidhardt FC, editor American Society for Microbiology.
8. Ignatova Z, Gierasch LM (2004) Monitoring protein stability and aggregation in vivo by real-time fluorescent labeling. Proc Natl Acad Sci U S A 101: 523–528. Available: http://www.pubmedcentral.nih.gov/articlerender.fcgi?artid = 327180&tool = pmcentrez&rendertype = abstract.
9. Ignatova Z, Krishnan B, Bombardier JP, Marcelino AMC, Hong J, et al. (2007) From the test tube to the cell: exploring the folding and aggregation of a beta-clam protein. Biopolymers 88: 157–163. Available: http://www.pubmedcentral.nih.gov/articlerender.fcgi?artid = 2904568&tool = pmcentrez&rendertype = abstract.
10. Li C, Pielak GJ (2009) Using NMR to distinguish viscosity effects from nonspecific protein binding under crowded conditions. J Am Chem Soc 131: 1368–1369. Available: http://www.pubmedcentral.nih.gov/articlerender.fcgi?artid = 2645536&tool = pmcentrez&rendertype = abstract.
11. McGuffee SR, Elcock AH (2010) Diffusion, crowding & protein stability in a dynamic molecular model of the bacterial cytoplasm. PLoS Comput Biol 6: e1000694. Available: http://www.pubmedcentral.nih.gov/articlerender.fcgi?artid = 2832674&tool = pmcentrez&rendertype = abstract.
12. Miklos AC, Sarkar M, Wang Y, Pielak GJ (2011) Protein crowding tunes protein stability. J Am Chem Soc 133: 7116–7120. Available:http://www.ncbi.nlm.nih.gov/pubmed/21506571.
13. Miklos AC, Li C, Sharaf NG, Pielak GJ (2010) Volume exclusion and soft interaction effects on protein stability under crowded conditions. Biochemistry 49: 6984–6991. Available: http://www.pubmedcentral.nih.gov/articlerender.fcgi?artid = 2927838&tool = pmcentrez&rendertype = abstract.
14. Schlesinger AP, Wang Y, Tadeo X, Millet O, Pielak GJ (2011) Macromolecular crowding fails to fold a globular protein in cells. J Am Chem Soc 133: 8082–8085. Available: http://www.pubmedcentral.nih.gov/articlerender.fcgi?artid = 3102155&tool = pmcentrez&rendertype = abstract.
15. Wang Q, Zhuravleva A, Gierasch LM (2011) Exploring weak, transient protein-protein interactions in crowded in vivo environments by in-cell nuclear magnetic resonance spectroscopy. Biochemistry 50: 9225–9236. Available: http://www.ncbi.nlm.nih.gov/pubmed/21942871.
16. Schnell S, Turner TE (2004) Reaction kinetics in intracellular environments with macromolecular crowding: simulations and rate laws. Prog Biophys Mol Biol 85: 235–260. Available: http://www.ncbi.nlm.nih.gov/pubmed/15142746.
17. Homchaudhuri L, Sarma N, Swaminathan R (2006) Effect of crowding by dextrans and Ficolls on the rate of alkaline phosphatase-catalyzed hydrolysis: a size-dependent investigation. Biopolymers 83: 477–486. Available: http://www.ncbi.nlm.nih.gov/pubmed/16868935.
18. Olsen SN (2006) Applications of isothermal titration calorimetry to measure enzyme kinetics and activity in complex solutions. Thermochimica Acta 448: 12–18. Available: http://linkinghub.elsevier.com/retrieve/pii/S0040603106003522.
19. Bodart J-F, Wieruszeski J-M, Amniai L, Leroy A, Landrieu I, et al. (2008) NMR observation of Tau in Xenopus oocytes. J Magn Reson 192: 252–257. Available: http://www.ncbi.nlm.nih.gov/pubmed/18378475.
20. Reckel S, Hansel R, Lohr F, Dötsch V (2007) In-cell NMR spectroscopy. Prog NMR Spectr 51: 91–101. Available: http://linkinghub.elsevier.com/retrieve/pii/S0079656507000076.
21. Sakai T, Tochio H, Tenno T, Ito Y, Kokubo T, et al. (2006) In-cell NMR spectroscopy of proteins inside Xenopus laevis oocytes. J Biomol NMR 36: 179–188. Available: http://www.ncbi.nlm.nih.gov/pubmed/17031531.
22. Sakakibara D, Sasaki A, Ikeya T, Hamatsu J, Hanashima T, et al. (2009) Protein structure determination in living cells by in-cell NMR spectroscopy. Nature 458: 102–105. Available: http://www.ncbi.nlm.nih.gov/pubmed/19262674.
23. Selenko P, Serber Z, Gadea B, Ruderman J, Wagner G (2006) Quantitative NMR analysis of the protein G B1 domain in Xenopus laevis egg extracts and intact oocytes. Proc Natl Acad Sci U S A 103: 11904–11909. Available: http://www.pubmedcentral.nih.gov/articlerender.fcgi?artid = 1523310&tool = pmcentrez&rendertype = abstract.
24. Serber Z, Keatinge-Clay T, Ledwidge R, Kelly AE, Miller SM, et al. (2001) High-resolution macromolecular NMR spectroscopy inside living cells. J Am Chem Soc 123: 2446–2447. Available: http://www.ncbi.nlm.nih.gov/pubmed/11456903.

25. Serber Z, Dötsch V (2001) In-Cell NMR Spectroscopy. Biochemistry 40: 14317–14323. Available: http://pubs.acs.org/doi/abs/10.1021/bi011751w.
26. Serber Z, Straub W, Corsini L, Nomura AM, Shimba N, et al. (2004) Methyl groups as probes for proteins and complexes in in-cell NMR experiments. J Am Chem Soc 126: 7119–7125. Available: http://www.ncbi.nlm.nih.gov/pubmed/15174883.
27. Wang Y, Li C, Pielak GJ (2010) Effects of proteins on protein diffusion. J Am Chem Soc 132: 9392–9397. Available: http://www.pubmedcentral.nih.gov/articlerender.fcgi?artid = 2898919&tool = pmcentrez&rendertype = abstract.
28. Crowley PB, Chow E, Papkovskaia T (2011) Protein interactions in the Escherichia coli cytosol: an impediment to in-cell NMR spectroscopy. Chembiochem 12: 1043–1048. Available: http://www.ncbi.nlm.nih.gov/pubmed/21448871.
29. Waudby CA, Mantle MD, Cabrita LD, Gladden LF, Dobson CM, et al. (2012) Rapid Distinction of Intracellular and Extracellular Proteins Using NMR Diffusion Measurements. J Am Chem Soc. 134:11312–11215. Available: http://www.ncbi.nlm.nih.gov/pubmed/22694283.
30. Janin J, Miller S, Chothia C (1988) Surface, subunit interfaces and interior of oligomeric proteins. J Mol Biol 204: 155–164. Available: http://www.ncbi.nlm.nih.gov/pubmed/3216390.
31. Tugarinov V, Kay LE (2006) A 2H NMR relaxation experiment for the measurement of the time scale of methyl side-chain dynamics in large proteins. J Am Chem Soc 128: 12484–12489. Available: http://www.ncbi.nlm.nih.gov/pubmed/16984199.
32. Tugarinov V, Ollerenshaw JE, Kay LE (2005) Probing side-chain dynamics in high molecular weight proteins by deuterium NMR spin relaxation: an application to an 82-kDa enzyme. J Am Chem Soc 127: 8214–8225. Available: http://www.ncbi.nlm.nih.gov/pubmed/15926851.
33. Carr H, Purcell E (1954) Effects of Diffusion on Free Precession in Nuclear Magnetic Resonance Experiments. Phys Rev 94: 630–638. Available: http://link.aps.org/doi/10.1103/PhysRev.94.630.
34. Meiboom S, Gill D (1958) Modified Spin-Echo Method for Measuring Nuclear Relaxation Times. Rev Sci Instrum 29: 688. Available: http://link.aip.org/link/RSINAK/v29/i8/p688/s1&Agg = doi.
35. Baldwin AJ, Religa TL, Hansen DF, Bouvignies G, Kay LE (2010) (13)CHD(2) methyl group probes of millisecond time scale exchange in proteins by (1)H relaxation dispersion: an application to proteasome gating residue dynamics. J Am Chem Soc 132: 10992–10995. Available: http://www.ncbi.nlm.nih.gov/pubmed/20698653.
36. Muhandiram DR, Yamazaki T, Sykes BD, Kay LE (1995) Measurement of 2H T1 and T1.rho. Relaxation Times in Uniformly 13C-Labeled and Fractionally 2H-Labeled Proteins in Solution. J Am Chem Soc 117: 11536–11544. Available: http://pubs.acs.org/doi/abs/10.1021/ja00151a018.
37. Barnes CO, Pielak GJ (2011) In-cell protein NMR and protein leakage. Proteins 79: 347–351. Available: http://www.pubmedcentral.nih.gov/articlerender.fcgi?artid = 3016450&tool = pmcentrez&rendertype = abstract.
38. Zhang M, Tanaka T, Ikura M (1995) Calcium-induced conformational transition revealed by the solution structure of apo calmodulin. Nat Struct Biol 2: 758–767. Available: http://www.ncbi.nlm.nih.gov/pubmed/7552747.
39. Kuboniwa H, Tjandra N, Grzesiek S, Ren H, Klee CB, et al. (1995) Solution structure of calcium-free calmodulin. Nat Struct Biol 2: 768–776. Available: http://www.biozentrum.unibas.ch/grzesiek/pdf/1995/Kuboniwa_NSB2_768.pdf.
40. Babu YS, Bugg CE, Cook WJ (1988) Structure of calmodulin refined at 2.2 Å resolution. J Mol Biol 204: 191–204. Available:http://www.ncbi.nlm.nih.gov/pubmed/1474585.
41. Siivari K, Zhang M, Palmer AG, Vogel HJ (1995) NMR studies of the methionine methyl groups in calmodulin. FEBS Lett 366: 104–108. Available: http://www.ncbi.nlm.nih.gov/pubmed/7789524.
42. Ikura M, Clore GM, Gronenborn AM, Zhu G, Klee CB, et al. (1992) Solution structure of a calmodulin-target peptide complex by multidimensional NMR. Science 256: 632–638. Available: http://www.ncbi.nlm.nih.gov/pubmed/1585175.
43. Hansen DF, Yang D, Feng H, Zhou Z, Wiesner S, et al. (2007) An exchange-free measure of 15N transverse relaxation: an NMR spectroscopy application to the study of a folding intermediate with pervasive chemical exchange. J Am Chem Soc 129: 11468–11479. Available: http://www.ncbi.nlm.nih.gov/pubmed/17722922.
44. Lipari G, Szabo A (1982) Model-free approach to the interpretation of nuclear magnetic resonance relaxation in macromolecules. 1. Theory and range of validity. J Am Chem Soc 104: 4546–4559. Available: http://pubs.acs.org/doi/abs/10.1021/ja00381a010.
45. Lipari G, Szabo A (1982) Model-free approach to the interpretation of nuclear magnetic resonance relaxation in macromolecules. 2. Analysis of experimental results. J Am Chem Soc 104: 4559–4570. Available: http://pubs.acs.org/doi/abs/10.1021/ja00381a010.
46. Mittermaier AK, Kay LE (1999) Measurement of Methyl 2 H Quadrupolar Couplings in Oriented Proteins. How Uniform Is the Quadrupolar Coupling Constant? J Am Chem Soc 121: 10608–10613. Available: http://pubs.acs.org/doi/abs/10.1021/ja9925047.
47. Goehlert VA, Krupinska E, Regan L, Stone MJ (2004) Analysis of side chain mobility among protein G B1 domain mutants with widely varying stabilities. Protein Sci 13: 3322–3330. Available: http://www.pubmedcentral.nih.gov/articlerender.fcgi?artid = 2287306&tool = pmcentrez&rendertype = abstract.
48. Igumenova TI, Frederick KK, Wand AJ (2006) Characterization of the fast dynamics of protein amino acid side chains using NMR relaxation in solution. Chem Rev 106: 1672–1699. Available: http://www.pubmedcentral.nih.gov/articlerender.fcgi?artid = 2547146&tool = pmcentrez&rendertype = abstract.
49. Skrynnikov NR, Millet O, Kay LE (2002) Deuterium spin probes of side-chain dynamics in proteins. 2. Spectral density mapping and identification of nanosecond time-scale side-chain motions. J Am Chem Soc 124: 6449–6460. Available: http://www.ncbi.nlm.nih.gov/pubmed/12033876.
50. Tjandra N, Kuboniwa H, Ren H, Bax A (1995) Rotational dynamics of calcium-free calmodulin studied by 15N-NMR relaxation measurements. Eur J Biochem 230: 1014–1024. Available: http://www.ncbi.nlm.nih.gov/pubmed/7601131.
51. Lee AL, Kinnear SA, Wand AJ (2000) Redistribution and loss of side chain entropy upon formation of a calmodulin-peptide complex. Nat Struct Biol 7: 72–77. Available: http://www.ncbi.nlm.nih.gov/pubmed/10625431.
52. Beece D, Eisenstein L, Frauenfelder H, Good D, Marden M, et al. (1980) Solvent viscosity and protein dynamics. Biochemistry 19: 5147–5157. Available: http://pubs.acs.org/doi/abs/10.1021/bi00564a001.
53. Vitkup D, Ringe D, Petsko GA, Karplus M (2000) Solvent mobility and the protein "glass" transition. Nat Struct Biol 7: 34–38. Available: http://www.ncbi.nlm.nih.gov/pubmed/10625424.
54. Fenimore PW, Frauenfelder H, McMahon BH, Parak FG (2002) Slaving: solvent fluctuations dominate protein dynamics and functions. Proc Natl Acad Sci U S A 99: 16047–16051. Available: http://www.pubmedcentral.nih.gov/articlerender.fcgi?artid = 138562&tool = pmcentrez&rendertype = abstract.
55. Young RD, Fenimore PW (2011) Coupling of protein and environment fluctuations. Biochim Biophys Acta 1814: 916–921. Available:http://www.ncbi.nlm.nih.gov/pubmed/21621015.
56. Doster W (2010) The protein-solvent glass transition. Biochim Biophys Acta 1804: 3–14. Available: http://www.ncbi.nlm.nih.gov/pubmed/19577666.
57. Persson E, Halle B (2008) Cell water dynamics on multiple time scales. Proc Natl Acad Sci U S A 105: 6266–6271. Available: http://www.pubmedcentral.nih.gov/articlerender.fcgi?artid = 2359779&tool = pmcentrez&rendertype = abstract.
58. Lundström P, Vallurupalli P, Religa TL, Dahlquist FW, Kay LE (2007) A single-quantum methyl 13C-relaxation dispersion experiment with improved sensitivity. J Biomol NMR 38: 79–88. Available: http://www.ncbi.nlm.nih.gov/pubmed/17464570.
59. Hansen DF, Vallurupalli P, Lundström P, Neudecker P, Kay LE (2008) Probing chemical shifts of invisible states of proteins with relaxation dispersion NMR spectroscopy: how well can we do? J Am Chem Soc 130: 2667–2675. Available: http://www.ncbi.nlm.nih.gov/pubmed/18237174.
60. Millet O, Loria JP, Kroenke CD, Pons M, Palmer AG (2000) The Static Magnetic Field Dependence of Chemical Exchange Linebroadening Defines the NMR Chemical Shift Time Scale. J Am Chem Soc 122: 2867–2877. Available: http://pubs.acs.org/doi/abs/10.1021/ja993511y.
61. Gilli R, Lafitte D, Lopez C, Kilhoffer M, Makarov A, et al. (1998) Thermodynamic analysis of calcium and magnesium binding to calmodulin. Biochemistry 37: 5450–5456. Available: http://www.ncbi.nlm.nih.gov/pubmed/9548926.
62. Homouz D, Sanabria H, Waxham MN, Cheung MS (2009) Modulation of calmodulin plasticity by the effect of macromolecular crowding. J Mol Biol 391: 933–943. Available: http://www.pubmedcentral.nih.gov/articlerender.fcgi?artid = 2728162&tool = pmcentrez&rendertype = abstract.
63. Wang Q, Liang K-C, Czader A, Waxham MN, Cheung MS (2011) The effect of macromolecular crowding, ionic strength and calcium binding on calmodulin dynamics. PLoS Comput Biol 7: e1002114. Available: http://dx.plos.org/10.1371/journal.pcbi.1002114.
64. Vold RR, Vold RL (1991) Advances in magnetic and optical resonance. 16th ed. Warren WS, editor Academic Press.
65. Evenäs J, Malmendal A, Akke M (2001) Dynamics of the transition between open and closed conformations in a calmodulin C-terminal domain mutant. Structure 9: 185–195. Available: http://www.ncbi.nlm.nih.gov/pubmed/11286885.
66. Tugarinov V, Kanelis V, Kay LE (2006) Isotope labeling strategies for the study of high-molecular-weight proteins by solution NMR spectroscopy. Nat Protoc 1: 749–754. Available: http://www.ncbi.nlm.nih.gov/pubmed/17406304.
67. Luby-Phelps K (2000) Cytoarchitecture and physical properties of cytoplasm: volume, viscosity, diffusion, intracellular surface area. Int Rev Cytol 192: 189–221. Available: http://www.ncbi.nlm.nih.gov/pubmed/10553280.
68. Zimmerman SB, Trach SO (1991) Estimation of macromolecule concentrations and excluded volume effects for the cytoplasm of Escherichia coli. J Mol Biol 222: 599–620. Available: http://www.ncbi.nlm.nih.gov/pubmed/1748995.
69. Fulton AB (1982) How crowded is the cytoplasm? Cell 30: 345–347. Available: http://www.ncbi.nlm.nih.gov/pubmed/6754085.
70. Press WH, Flannery BP, Teukolsky SA, Vetterling WT (1992) Numerical Recipes in C: The Art of Scientific Computing. 2nd Editio. Cambridge University Press.
71. Delaglio F, Grzesiek S, Vuister GW, Zhu G, Pfeifer J, et al. (1995) NMRPipe: a multidimensional spectral processing system based on UNIX pipes. J Biomol NMR 6: 277–293. Available: http://www.ncbi.nlm.nih.gov/pubmed/8520220.
72. Vallurupalli P, Hansen DF, Stollar E, Meirovitch E, Kay LE (2007) Measurement of bond vector orientations in invisible excited states of proteins. Proc Natl Acad Sci U S A 104: 18473–18477. Available: http://www.pubmedcentral.nih.gov/articlerender.fcgi?artid = 2141801&tool = pmcentrez&rendertype = abstract.